HHS Public Access

Author manuscript

Mol Cancer Ther. Author manuscript; available in PMC 2020 August 01.

Published in final edited form as:

Mol Cancer Ther. 2020 February ; 19(2): 348–363. doi:10.1158/1535-7163.MCT-19-0536.

An orally available tubulin inhibitor, VERU-111, suppresses triple-negative breast cancer tumor growth and metastasis and bypasses taxane resistance

Shanshan Deng[‡,1], **Raisa I Krutilina**[‡,2], **Qinghui Wang**[1], **Zongtao Lin**[1], **Deanna N. Parke**[2], **Hilaire C. Playa**[2], **Hao Chen**[1], **Duane D. Miller**[1], **Tiffany N. Seagroves**[1,2,*], **Wei Li**[1,*]

[1]Department of Pharmaceutical Sciences, College of Pharmacy, University of Tennessee Health Science Center, Memphis, TN38163, United States

[2]Department of Pathology, College of Medicine, University of Tennessee Health Science Center, Memphis, TN38103, United States.

Abstract

Triple-negative breast cancer (TNBC) accounts for ~15% of breast cancer cases in the United States. TNBC has poorer overall prognosis relative to other molecular subtypes due to rapid onset of drug resistance to conventional chemotherapies and increased risk of visceral metastases. Taxanes like paclitaxel are standard chemotherapies that stabilize microtubules, but their clinical efficacy is often limited by drug resistance and neurotoxicities. We evaluated the preclinical efficacy of a novel, potent and orally bioavailable tubulin inhibitor, VERU-111, in TNBC models. VERU-111 showed potent cytotoxicity against TNBC cell lines, inducing apoptosis and cell cycle arrest in a concentration-dependent manner. VERU-111 also efficiently inhibited colony formation, cell migration and invasion. Orally administered VERU-111 inhibited MDA-MB-231 xenograft growth in a dose-dependent manner, with similar efficacies to paclitaxel, but without acute toxicity. VERU-111 significantly reduced metastases originating from the mammary fat pad and lung, liver and kidney metastasis in an experimental metastasis model. Moreover, VERU-111, but not paclitaxel, suppressed growth of luciferase-labeled, taxane-resistant patient-derived metastatic TNBC tumors. In this model, VERU-111 repressed growth of pre-established axillary lymph node metastases and lung, bone and liver metastases at study endpoint, whereas paclitaxel enhanced liver metastases relative to vehicle controls. Collectively, these studies strongly suggest that VERU-111 is not only a potent inhibitor of aggressive TNBC phenotypes, but it is also

[*]**Corresponding authors:** Wei Li, Ph.D., Address: 881 Madison Avenue, room 561, Memphis, TN 38163. Phone: 901-448-7532, wli@uthsc.edu, Tiffany N. Seagroves, Ph.D., Address: 19 South Manassas Street, Cancer Research Building, room 262, Memphis, TN 38163. Phone: 901-448-5018, tseagro1@uthsc.edu.

[‡]Equal contributions

Authors' Contributions

Conception and design: S. Deng, R.I. Krutilina, T.N. Seagroves, W. Li

Development of methodology: S. Deng, R.I. Krutilina, D. N. Parke, H.C. Barch, T.N. Seagroves, W. Li

Acquisition of data: S. Deng, R.I. Krutilina, Q. Wang, Z. Lin, H.C. Barch, H. Chen, T.N. Seagroves

Analysis and interpretation of data: S. Deng, R.I. Krutilina, D. N. Parke, H.C. Barch, D. D. Miller, T.N. Seagroves, W. Li

Writing, review, and/or revision of the manuscript: S. Deng, R.I. Krutilina, Q. Wang, Z. Lin, H.C. Barch, D. D. Miller, T.N. Seagroves, W. Li

Administrative, technical, or material support: T.N. Seagroves, W. Li

Study supervision: T.N. Seagroves, W. Li

Other (chemical design and synthesis): Q. Wang, H. Chen

efficacious in a taxane-resistant model of metastatic TNBC. Thus, VERU-111 is a promising new generation of tubulin inhibitor for the treatment of TNBC and may be effective in patients who progress on taxanes.

Keywords

TNBC; anti-mitotic agents; microtubules; proliferation; metastasis

Introduction

Breast cancer is the second leading cause of cancer-related deaths in women in the United States, leading to approximately 40,920 deaths in 2017 (1). Approximately 15% of all breast cancer cases are classified as the TNBC subtype, characterized by the absence of estrogen receptor, progesterone receptor and human epidermal growth factor 2 (HER2) (2). Conventional endocrine therapy or HER2-targeted therapy is effective for the hormone receptor positive or HER2 positive breast cancers, but not for TNBC due to the lack of targets (3,4). Thus, cytotoxic chemotherapy is still a primary treatment regimen for TNBC patients. TNBC is highly aggressive and is characterized by poor prognosis due to relatively quick relapse after chemotherapy (5,6), with enhanced rates of visceral metastasis. Therefore, there is an urgent need to develop novel effective therapeutics for the treatment of TNBC, particularly for chemorefractory disease.

Microtubules, composed of α- and β-tubulin heterodimers, are important for cell structure maintenance, cell mitosis and intracellular transport (7). Interference with microtubule assembly arrests cell cycle progression, and ultimately induction of cell death, making microtubules an attractive target in anticancer drug discovery (8,9). At least four major binding sites on the microtubules for anti-mitotic agents have been discovered: taxol-binding site, vincristine-binding site, colchicine-binding site and laulimalide-binding site (10). Existing tubulin inhibitors, such as paclitaxel, are highly successful in breast cancer treatment, however, due to poor aqueous solubility, they must be IV-infused. In addition, their clinical use is often limited by drug resistance mediated by ATP-binding cassette (ABC) transporters and neurotoxicities (11–13). Extensive preclinical studies have suggested that tubulin inhibitors targeting the colchicine-binding site are significantly less vulnerable to transporter-mediated drug resistance, and several of these agents have been tested in clinical trials (10,14). However, up to this point, none of these colchicine binding site inhibitors (CBSIs) have gained FDA-approval, mainly due to toxicities and their lack of clinical benefit. While targeting tubulin polymerization may involve inherent toxicity, for many of these CBSIs, the major toxicities that led to clinical failures are related to their specific chemical structures (15,16). Developing a new generation of CBSI with a unique chemical structure that possesses a good therapeutic index could lead to a new anticancer agent for safe and effective chemotherapy, particularly for metastatic disease.

A series of novel compounds that target the colchicine-binding site, termed ABI-III chemotypes, were designed and synthesized based on our previously reported 2-aryl-4-benzoyl-imidazole analogues (17). These ABI-III analogues possessed nanomolar

cytotoxicity against a panel of melanoma and prostate cancer cell lines and they overcame multidrug resistance mediated by the ABC transporter P-glycoprotein (P-gp) (17). Among these, VERU-111, also named ABI-231, showed the most potent anti-proliferative activity against five melanoma and prostate cancer cell lines and is the clinical candidate for trials for advanced prostate cancer (). Oral activity and efficacy of VERU-111 were previously evaluated in paclitaxel- or docetaxel-resistant tumor models; VERU-111 has favorable pharmacokinetic properties with acceptable oral bioavailability, ranging from 21% to 50%, in mice, rats and dogs (18). Therefore, we investigated the antitumor activity of VERU-111 specifically for the treatment of metastatic TNBC. The *in vitro* efficacy of VERU-111 was assayed using two conventional TNBC cell lines (MDA-MB-231 and MDA-MB-468) and two luciferase-labeled TNBC primary cell lines derived from metastatic patient-derived xenograft (PDX) models created at the Huntsman Cancer Institute (HCI) (19), HCI-2-Luc2 (treatment-naïve) and HCI-10-Luc2 (taxane refractory). VERU-111 had potent anti-proliferative activity against all models tested, including the taxane-resistant HCI-10 model (low nM range). Furthermore, VERU-111 inhibited cancer cell colony formation, cell migration and invasion, likely through the anti-proliferative related mechanisms regulating microtubule assembly, G2/M cell cycle arrest and induction of apoptosis. In a MDA-MB-231 xenograft model, orally administered VERU-111 inhibited TNBC xenograft tumor growth in a dose-dependent manner with antitumor potency similar to paclitaxel and repressed visceral metastasis in both an orthotopic setting and in an experimental metastasis model. VERU-111, but not paclitaxel, significantly repressed primary tumor growth, growth of pre-established axillary lymph node metastases and repressed endpoint metastasis in mice bearing HCI-10-Luc2 xenografts derived from the PDX model (20). Collectively, these data position VERU-111 as a promising drug candidate for the more effective treatment of metastatic TNBC, potentially including patients who progress on taxanes.

Materials and Methods

Chemical compounds and cell lines

Colchicine was purchased from Sigma-Aldrich (St. Louis, MO). Paclitaxel was purchased from LC Laboratories (Woburn, MA). VERU-111 was synthesized by a reported method (21), purity (⩾98%) and identity were verified by HPLC, HR-MS (Waters, Milford, MA) and proton nuclear magnetic resonance (Bruker, Billerica, MA). MDA-MB-231 and MDA-MB-468, were purchased from ATCC (Manassas, VA) and authenticated prior to use and then every year at the University of Arizona Genetics Core. Cells were cultured in DMEM-Hi (Mediatech, Inc., Manassas, VA) supplemented with 10% fetal bovine serum (Atlanta Biologicals, Lawrenceville, GA) and 1% antibiotic-antimycotic solution (Sigma-Aldrich) at 37°C in a humidified atmosphere containing 5% CO_2. Spent media was routinely tested for mycoplasma using the MycoAlert kit (Lonza). The parental HCI-2 and HCI-10 patient-derived xenograft (PDX) breast tumor lines (TNBC: ER−/PR−/HER2−) were originally provided by Dr. Alana Welm and the Huntsman Cancer Institute (HCI) tissue resource and application core (19). HCI-2-Luc2 and HCI-10-Luc2 patient-derived tumor xenograft lines were developed by transient cell culture of parent primary PDX tumor cells in stem cell conditions with a lentivirus expressing luciferase-2 and puromycin, followed by transplant into and exclusive passage in immunocompromised recipient mice, as described in (20).

Primary cell lines generated from the Luc2-labeled tumor xenografts were grown in adherent conventional cell culture conditions and were maintained in M87 growth medium as in (19,20). Luciferase-labeled HCI PDX-derived primary cell lines and subsequent tumor xenograft material were authenticated by matching to the original deidentified patient sample by whole genome expression profiling at the Huntsman Cancer Institute.

Cell growth inhibition assay

A MTS assay was used to score for cell growth inhibition effects of an increasing concentration range of colchicine, paclitaxel and VERU-111 in human melanoma (A375 and M14), human HER2-positive breast (SKBR3) and TNBC (MDA-MB-231, MDA-MB-453 and MDA-MB-468) cell lines for 72 h as described previously (21). HCI-2- or HCI-10-Luc2 patient-derived primary cell lines were seeded at 20,000 cells/well and grown in the presence of drugs for six days. Drug response was normalized to untreated and vehicle-only controls, plotted on log scale and analyzed using non-linear regression best fit analysis modules in Prism 7.0. For all cell models, at least three biological replicate experiments were averaged to calculate the grand mean IC_{50} ± SEM.

Colony formation assay

MDA-MB-231 or MDA-MB-468 cells were seeded into 12-well plates (250 or 500 cells/well, respectively) and then treated 24 h later with increasing concentrations of colchicine, paclitaxel and VERU (8, 16 or 32 nM). Medium was replaced with fresh drug once per week. Cells were fixed with methanol and stained with 0.5% crystal violet and colony morphology was visualized by a microscope and colonies quantified using ImageJ software (NIH, Bethesda, MD).

Immunofluorescence staining

MDA-MB-231 (1×10^5) or MDA-MB-468 (2×10^5) cells were seeded in 6-well plates onto sterile coverslips for 24 h prior to treatment with 16 nM of colchicine, paclitaxel or VERU-111 for 18 h. For tubulin visualization, cells were washed with PBS, fixed with 4% paraformaldehyde for 15 min and permeabilized with 0.2% Triton X-100/PBS for 15 min. Following blocking in 1.5% bovine serum albumin (BSA), 0.1% Tween 20 in PBS for 1 h, coverslips were incubated with anti-α-tubulin antibody (Thermo Fisher Scientific, Rockford, IL) in 1% BSA/0.1% Tween 20/PBS overnight at 4 °C. Cells were then washed and incubated with Alexa Fluor 647 goat anti-mouse IgG (Molecular Probes, Eugene, OR) for 1 h at room temperature, mounted with Prolong Diamond Antifade containing DAPI (Invitrogen, Eugene, OR), and images captured with a Keyence BZ-X700 microscope (Itasca, IL).

Cell migration and invasion assay

Cell migration and invasion were measured, respectively, using transwell 24-well plates with a non-coated membrane insert (pore size 8μm) or a Matrigel-coated insert (BD Biosciences, CA). MDA-MB-231 and MDA-MB-468 cells were starved in serum-free medium for 24 h followed by suspension of the cells (MDA-MB-231: 4×10^4 and MDA-MB-468:10^5) in serum-free medium containing 8 nM of VERU-111 and then plating in the top chamber of

the inserts. Medium containing 10% FBS was added to the lower chamber as a chemoattractant and cells were incubated for 24 h (MDA-MB-231) or 48 h (MDA-MB-468). The chambers were fixed in cold methanol, stained with 0.5% crystal violet and imaged. The number of migrating or invading cells was counted using ImageJ software and normalized to the control group for each cell line (as 100%). Random cell migration was then analyzed by a manual scratch wound healing assay. MDA-MB-231 cells (10^5 cells/well) and MDA-MB-468 (2×10^5 cells/well) cells were seeded in 12-well plates and allowed to adhere overnight. The following day, a scratch was made in the confluent cell monolayer using a sterile 200 μL pipette tip. The cell culture medium was replaced by medium containing vehicle (DMSO), colchicine, paclitaxel or VERU-111 (16 nM). At 12, 24 and 48 h, wound width was imaged with an Evos Fl Imaging System (Life Technologies, Carlsbad, CA) and closure expressed relative to the size of the original scratch width at each measured time point in the drug-treated wells relative to the vehicle control.

Cell cycle analysis

After treatment with each drug, cells were harvested by trypsinization, fixed, permeabilized, stained with anti-phospho-histone H3 (Ser 10)-AlexaFluor® 488 antibody on ice for 1 h and then incubated with freshly prepared propidium iodide/RNase solution for 30 min at room temperature per the manufacturer's protocol (#FCCH025103, EMD Millipore Corporation, Burlington, MA). Stained cells were analyzed using a Bio-Rad ZE5 instrument (Bio-Rad, Hercules, CA) and data were analyzed using FlowJo version 10 (FlowJo, LLC, Ashland, OR) in the University of Tennessee Health Science Center (UTHSC) Flow Cytometry and Cell Sorting core. First, total cells were gated, followed by gating out cell doublets and debris. Cells in sub G1, G1, S and G2 phases were then gated according to DNA content, as determined from histogram plots of PI staining-Area. Cell populations were defined and analyzed from the bottom half of G1 peak, middle of the S phase and the top half of G2 peak, respectively. Cells in M phase were identified by comparing the compensation control sample with the Phospho-Histone H3-AlexaFluor® 488 stained samples and gated only for phosphor-histone H3 stained cells.

Detection of apoptosis

MDA-MB-231 and MDA-MB-468 cells were seeded in 6-well plates (2×10^5/well). The next day, cells were treated with 100 nM of VERU-111 for 24, 48 or 72 h. Alternatively, cells were treated with increasing concentrations of VERU-111 for 24 h. At harvest, 10^5 cells were suspended in 185 μL of Annexin-V-FITC binding buffer (eBioscience, Grand Island, NY) and 5 μL of Annexin-V-FITC (eBioscience) and 10 μL propidium iodide were added, followed by incubation for 10 min at room temperature (RT), and analysis in the UTHSC Flow Cytometry and Cell Sorting core.

Caspase 3/7 activity assay

Apoptosis induced by VERU-111 was measured using the Caspase Glo 3/7 assay system (Promega, Madison, WI) (22). Cells (5,000 cells/well) were seeded into a 96-well plate and treated with either colchicine, paclitaxel or VERU-111 (20 nM) for 24 h, and caspase 3/7 activity was normalized by total protein content.

Western blotting

Cells grown to 70% confluence were incubated with increasing concentrations of VERU-111 or 100 nM colchicine or paclitaxel for 24 h. For time-dependent studies, cells were exposed to 100 nM VERU-111 for 24, 48 or 72 h. For P-gp detection, PDX cells were collected at 70% confluence. At harvest, cells were washed with ice-cold PBS, lysed in RIPA buffer (25 mM Tris pH 7.6, 150 mM NaCl, 1% NP-40, 1% sodium deoxycholate, 0.1% SDS) in the presence of Halt™ protease and phosphatase inhibitor (Thermo Fisher Scientific) and centrifuged at 13,000 rpm at 4 °C for 10 min. Protein concentration was determined by the BCA Protein Assay (Thermo Fisher Scientific). Denatured protein samples were separated by SDS-PAGE gradient gels (Bio-Rad, #456–1083) and transferred to PVDF membrane. Membranes were blocked in 5% non-fat milk in TBST solution at RT for 1 h, incubated with primary antibodies overnight at 4 °C and incubated with secondary antibody for 1 h (1:2000, either #7074 or #7076, Cell Signaling Technology, Danvers, MA). Primary antibodies included: rabbit anti-cleaved PARP (1:1000), rabbit anti-cleaved-caspase-3 (1:1000), rabbit anti-GAPDH HRP conjugate (#9532; #5625; #9661; #3683, respectively, Cell Signaling Technology) and mouse anti-P-gp (MA1–26528, Thermo Fisher Scientific). Proteins were detected using Clarity™ Western ECL Substrate (Bio-Rad, #1705060) and visualized by the ChemiDoc-It2 Imager system (UVP, LCC, Upland, CA).

In vivo orthotopic MDA-MB-231 xenograft model

All protocols and methods were approved by the UTHSC Animal Care and Use Committee (ACUC), consistent with the *Guide for the Care and Use of Laboratory Animals*, 8th edition (protocols #17–080 and #17–056). Female Nod-Scid-Gamma (NSG) mice at 5–6 weeks of age were housed with a 12:12-hour light-dark cycle and fed a breeder chow diet. MDA-MB-231 cells suspended in 10 μL of HBSS (2.5×10^5) were surgically inoculated into the left and the right inguinal mammary gland fat pads of deeply anesthetized NSG mice using a Hamilton syringe mounted with a ½” 26G PT2 point needle as in (23). Mice were palpated and measured with digital calipers weekly until the average tumor size per mouse was 100 mm^3. Mice were then randomly divided into 5 groups such that the mean tumor volumes were equivalent across cohorts (Cohort 1: vehicle, 1:1 ratio of PEG 300:water, PO, n = 14 mice; Cohort 2: 5 mg/kg VERU-111, PO, n = 8 mice; Cohort 3: 10 mg/kg VERU-111, PO, n = 8 mice; Cohort 4: 12.5 mg/kg VERU-111, PO, n = 8 mice; Cohort 5: 12.5 mg/kg paclitaxel, IP, n = 8 mice). Animals in the vehicle and VERU-111 MDA-MB-231 xenograft cohorts were dosed orally (PO) five times per week (Monday-Friday) and animals treated with paclitaxel were dosed every other day (IP). Primary tumor size was monitored twice a week and the body weight of the mice was recorded daily. Tumor volume was calculated by the formula volume = (width^2 × length)/2. All animals were euthanized when total tumor volume in the vehicle control group exceeded 1000 mm^3 (after 18 days on therapy). Excised tumors were photographed, and final tumor volume was calculated from *ex vivo* caliper measurements. Tumors were then divided in half and either flash frozen or fixed overnight at room temperature in buffered formalin. Lungs were harvested after inflation with saline and post-fixed in formalin overnight prior to downstream histological analysis using the UTHSC Research Histology Core.

Experimental lung metastasis model

NSG female mice (7–8 weeks old) were injected with 2×10^5 MDA-MB-231 cells in 100 μL of HBSS via tail vein. Twenty-four hours later, mice were treated with either vehicle, 10 mg/kg of VERU-111 or 10 mg/kg paclitaxel (n = 7 mice/group) using the same dosing regimen as the orthotopic xenograft model. Body weight was monitored weekly. After 23 days, mice were sacrificed, and lungs, livers, kidneys, spleens were photographed and then fixed in formalin overnight.

Histology and immunohistochemistry (IHC) analysis

Fixed tumors and organs were embedded in paraffin and unstained slides were prepared for immunostaining or stained with H&E. IHC staining was performed as previously described (21). Primary antibodies included rabbit anti-Ki67 (1:400), rabbit anti-CD31 (1:100) (#9027; #77699, Cell Signaling Technology), rabbit anti-cleaved PARP (1:50) and rabbit anti-cleaved-caspase-3 (1:200), detected by a biotinylated horse anti-rabbit IgG antibody (BA-1100, Vector Laboratories Inc., Burlingame, CA) secondary antibody. Anti-human-specific mitochondria IHC staining (AbCAM, Cambridge, MA, cat# ab92824) was performed at a 1:1000 dilution to visualize metastases. All slides were developed with DAB Impact (Vector Labs, Burlingame, CA), counterstained in Gill's hematoxylin (Vector Labs) and mounted with Cytoseal XYL mounting media. Tissue images were acquired with a Keyence BZ-X700 microscope. Quantification of metastatic burden was performed by digital scanning of whole stained slides using a Pannoramic FLASH III system (3D Histech), followed by manual counting of metastatic lesions present in the tissue section. Quantification of Ki67-, CD31-, cleaved-PARP- and cleaved-caspase-3-positive tumor cells was performed by calculating the area of positive cells in 4–5 representative fields per section using the Keyence Hybrid Cell Count module.

Patient-derived xenograft models

The parental HCI-10 PDX model was originally derived from a pleural effusion of a heavily-treated patient diagnosed with metastatic breast cancer (19). To facilitate whole-body bioluminescent imaging, this model was previously labeled with firefly luciferase as described (20). After transient cell culture in stem cell culture conditions to achieve viral transduction and reporter labeling, HCI-10-Luc2 cells were implanted into a donor female NSG mouse and then serially re-transplanted and/or cryopreserved to maintain the line. Tumor fragments from a donor tumor-bearing mouse were bilaterally implanted into the cleared inguinal mammary fat pads of recipient NSG female mice (4–6 weeks of age). Primary tumor growth and metastasis were monitored bi-weekly by caliper measurement and bio-imaging (Perkin Elmer XMRS) (1x/week) beginning two weeks post-surgery. Body weights were recorded every other day. As soon as one tumor per mouse grew to ~100 mm^3, mice were randomized such that mean tumor volumes were equivalent in each cohort: Cohort 1: vehicle (PO, five consecutive days/week, n = 12 mice), Cohort 2: 10 mg/kg paclitaxel (IV, 1x/week, n = 13 mice) and Cohort 3: 10 mg/kg VERU-111 (PO, 5 consecutive days /week, n = 13 mice). Mice were then bio-imaged the day before treatment to screen for pre-existing AxLN metastases. All bio-imaging data are shown as total flux (photons/s), calculated using Living Image software. After 8 weeks on treatment, when

mean tumor volume in the vehicle control group was ~500 mm^3, all animals were euthanized. All organs were collected and bio-imaged *ex vivo* to confirm location of metastatic signals observed in intact mice and to quantitate metastatic burden specific to that organ. Collected tumors and organs were processed for histology as described above.

Statistical analysis

All data were analyzed using GraphPad Prism 7 (San Diego, CA). *In vitro* experiments were repeated using at least three technical replicates per group and each assay performed over three biological replicates. One-way or two-way ANOVA tests were first employed for experiments comparing more than two groups/conditions, followed by pairwise, two tailed Student's *t*-tests or a Dunnett's multiple comparison test. Student's *t*-tests were used to compare treatment group to the control group for the *in vitro* migration and invasion assays. One-way ANOVA analyses followed by the Dunnett's test was used to evaluate differences between treatments and controls for the *in vitro* colony formation, scratch and cell apoptosis detection assays, as well as all *in vivo* xenograft studies. Significance levels are defined as $*p < 0.05$, $**p < 0.01$, $***p < 0.001$, $****p < 0.0001$.

Results

VERU-111 attenuates proliferation of breast cancer cells and impairs microtubule assembly and mitotic spindle organization

VERU-111 (Fig. 1A) has an average IC_{50} of 4 nM in melanoma cells (17). We evaluated whether VERU-111 could inhibit the growth of HER2+ (SKBR3) and TNBC breast cancer cells (MDA-MB-231, −468 and −453 cells). VERU-111 had potent anti-proliferative effect in all cells, with IC_{50} values in the low nM range: SKBR3 (14 nM) and 8–14 nM in TNBC cells (Supplementary Table S1). The tubulin-destabilizing agent colchicine and the tubulin-stabilizing agent paclitaxel were then compared to VERU-111 using two TNBC cell lines (Fig. 1B). All three inhibitors inhibited cell proliferation. Mean IC_{50} values of colchicine, paclitaxel and VERU-111 ranged from 9.8–17.5 nM, 3.1–4.6 nM and 8.2–9.6 nM, respectively, depending on the model. VERU-111 reduced colony formation of TNBC cells in a concentration-dependent manner (Fig. 1C). In MDA-MB-231 cells, paclitaxel completely repressed colony formation at a concentration as low as 8 nM. In contrast, colony formation was reduced, but not eliminated, at an equivalent concentration of either colchicine or VERU-111, although 16 nM of VERU-111 was more effective than 16 nM of colchicine. Similar results were observed in MDA-MB-468 cells.

VERU-111 demonstrates robust antitumor activity by destabilizing tubulin polymerization through targeting the colchicine-binding site (17). Thus, we performed immunofluorescence staining to visualize the microtubule network after treatment with colchicine, VERU-111 and paclitaxel. Control cells showed intact microtubule fibers and typical microtubule organization (Fig. 1D). As expected, treatment with paclitaxel produced aggregation and condensation of microtubules due to increased tubulin polymerization. Similar to colchicine, cells treated with VERU-111 were smaller and the cell shape changed from spindle-like to round and irregular, and the microtubules were depolymerized, confirming that VERU-111 disrupts tubulin polymerization in TNBC cells.

VERU-111 inhibits TNBC cells migration and invasion

VERU-111 (8 nM) inhibited cell migration by 44% in MDA-MB-231 cells and by 37% in MDA-MB-468 cells relative to the control (set to 100%) (Fig. 2A). Likewise, VERU-111 reduced invasion through Matrigel membrane by 50% in MDA-MB-231 and by 45% in MDA-MB-468 cells (Fig. 2B). Similar results on invasion potential were obtained when cells were exposed to 16 nM of VERU-111 (Supplementary Fig. S1). VERU-111, colchicine and paclitaxel showed effective inhibition of wound healing in a scratch wound assay at 16 nM (Fig. 2C). After 24 h, the average rates of migration in colchicine, paclitaxel and VERU-111-treated MDA-MB-231 cells were 67.3%, 43.3% and 44.9%, respectively, relative to vehicle control (DMSO). Similarly, after 48 hours treatment, colchicine, paclitaxel and VERU-111 reduced the average migration of MDA-MB-468 cells by 15.8%, 14.5% and 17.9%, respectively. Images of wounds are shown in Supplementary Figure S2. We also verified that lowering the concentration of VERU-111 to 8 nM also inhibited wound healing in TNBC cells (Supplementary Fig. S3A–B). Finally, the ability of VERU-111 to inhibit wound healing in a concentration-dependent manner over time was shown using MDA-MB-231 cells grown in the IncuCyte S3 live cell imaging system (Supplementary Fig. S3C). In summary, although VERU-111 impaired cell migration, invasion and wound healing, it is not possible to rule out the impact of VERU-111-dependent effects on growth inhibition and/or cytotoxicity on these assays.

VERU-111 blocks TNBC cells at G2/M checkpoint and induces cell apoptosis

Microtubule disruption typically leads to the mitotic arrest of growing cells in metaphase, ultimately causing cell death (24,25). To examine whether VERU-111 induces cell cycle arrest, cells treated with 100 nM of colchicine or paclitaxel and increasing concentrations of VERU-111 for 24 h were profiled by flow cytometry. Each compound showed divergent effects on cell cycle progression in each cell line. In MDA-MB-231 cells, VERU-111 treatment induced a G2/M block in a concentration-dependent manner, with a concomitant reduction in cells in the G1 and S phases. Colchicine and paclitaxel, also arrested MDA-MB-231 cells in the G2 and M phases, as expected (Fig. 3A and Supplementary Fig. S4A). Likewise, VERU-111 induced a G2 phase arrest in MDA-MB-468 cells, reducing the population of cells G1, with little effect on the S phase. In contrast to VERU-111, paclitaxel arrested MDA-MB-468 cells in the G2 and M phases (Fig. 3A). VERU-111 treatment caused a significant G2/M accumulation at a concentration of 20 nM in MDA-MB-231 cells, and at 50 nM in MDA-MB-468 cells, with maximum accumulation observed in response to a concentration of 100 nM.

The potential of VERU-111 to induce apoptosis in TNBC cells was analyzed using Annexin-V-FITC/PI co-staining. VERU-111 initiated apoptotic cell death in a concentration-dependent manner, as indicated by the appearance of Annexin-V^+/PI^- cells, Annexin-V^+/PI^+ cells and Annexin-V^-/PI^+ cells (Fig. 3B and Supplementary Fig. S4B). The potency of VERU-111 to induce apoptosis was identical to colchicine but required a higher concentration for paclitaxel. MDA-MB-231 and MDA-MB-468 cells treated with 100 nM VERU-111 for 24, 48 and 72 h underwent apoptosis in a time-dependent manner as shown in Fig. 3C and Supplementary Fig. S4C.

Caspases and PARP play an important role in the initiation and execution of programmed cell death (26,27). To determine whether VERU-111 triggers apoptotic cell death through these pathways, expression of cleaved-caspase-3 and cleaved-PARP in TNBC cells treated by VERU-111 was analyzed by western blotting (Fig. 3D–E), revealing increased expression of cleaved-caspase-3 and cleaved-PARP in a concentration-dependent manner after 24 hours treatment, although cleavage was overall lower than in cells treated with paclitaxel. Colchicine also induced the upregulation of cleaved-caspase-3 and cleaved-PARP in MDA-MB-468 cells after 24 hours treatment (Fig. 3D). There was also a clear, time-dependent increase in cleaved-caspase-3 and cleaved-PARP expression after VERU-111 treatment (Fig. 3E). Caspase 3/7 activity was next evaluated in each cell line using the Caspase Glo 3/7 assay, including colchicine and paclitaxel as positive controls (Fig. 3F). VERU-111, colchicine and paclitaxel displayed up to 4-fold higher caspase 3/7 activity levels relative to the control, consistent with induction of apoptosis effectors shown in Fig. 3B–C.

VERU-111 inhibits TNBC primary tumor growth

We next tested the antitumor activity of VERU-111 in an orthotopic metastatic TNBC mouse model (MDA-MB-231). Since paclitaxel is one of the most widely used chemotherapeutics for stage IV breast cancer, we incorporated paclitaxel as the comparison treatment. NSG mice bearing MDA-MB-231 xenografts were treated with either vehicle, 5-, 10- or 12.5 mg/kg of VERU-111 (PO) or 12.5 mg/kg paclitaxel (IP). Relative to vehicle treated mice, mean tumor size was significantly decreased in the 10 mg/kg and 12.5 mg/kg VERU-111 cohorts and in the paclitaxel-treated groups, whereas VERU-111 given at 5 mg/kg showed less potent inhibition (Fig. 4A). No significant loss of body weight was observed in the VERU-111 treated groups, although 12.5 mg/kg dosing of VERU-111 did appear to inhibit the weight gain observed in the other treatment groups over the course of the treatment. In contrast, the body weight of mice in the paclitaxel treatment group was significantly decreased (−10%), suggesting an accumulated toxicity (Fig. 4B). Relative to controls, each dose of VERU-111 significantly reduced mean tumor volume and mean wet weight with the largest effect observed at 12.5 mg/kg (Fig. 4C–D). Moreover, VERU-111 had comparable efficacy to paclitaxel since there were no significant differences between the means of the two groups at the same dose (276.61 mm^3 vs. 254.32 mm^3) (Fig. 4C). Similar changes were observed when the mean final tumor weights were compared (Fig. 4D). Both VERU-111 and paclitaxel treatment significantly reduced overall tumor size as compared to the vehicle control (Fig. 4E).

VERU-111 induces tumor necrosis, anti-angiogenesis and apoptosis *in vivo*

Paraffin-embedded tumor sections were then stained with H&E and with Ki67, CD31, cleaved-PARP and cleaved-caspase-3 by IHC (Fig. 5A). As necrotic areas would be expected in the tumor centers due to hypoxia, all H&E and IHC pictures were imaged near the tumor margins. Both VERU-111 and paclitaxel treatment increased the number of necrotic tumor cells with pyknosis, indicated by the nuclear shrinkage (Fig. 5A). The percentage of tumor area occupied by necrotic cells was not statistically significant between vehicle and the 5 mg/kg dose of VERU-111 (Fig. 5B); however, necrosis significantly increased in response to 10 mg/kg or 12.5 mg/kg of VERU-111. Approximately half of tumor area in the 12.5 mg/kg VERU-111-treatment group was necrotic, which was

comparable to the necrotic area in response to paclitaxel (41.5%). All doses of VERU-111 treatment significantly decreased, in a dose-dependent manner, the number of Ki67-positive cells and CD31-positive cells relative to the vehicle-treated tumors. Paclitaxel has been previously shown to inhibit breast tumor angiogenesis (28). Therefore, *in vivo*, like paclitaxel, VERU-111 inhibited the proliferation of TNBC cells and disrupted the tumor vasculature (Fig. 5C–D). A dose-dependent increase in the percentage of cells expressing both cleaved-PARP and cleaved-caspase-3 was also observed, confirming that VERU-111 efficiently induces apoptosis *in vivo* (Fig. 5E–F). As expected, tumor growth suppression, tumor vasculature disruption and apoptotic cell death induction were also evident for the paclitaxel treatment group (Fig. 5C–5F). Overall, we conclude that the antitumor activity of VERU-111 is equivalent to paclitaxel *in vivo*, but without evidence of toxicity.

VERU-111 inhibits metastasis either from the mammary fat pad or in an experimental metastasis model

The lungs were harvested from the same cohort of MDA-MB-231 mammary-tumor bearing mice shown in Fig. 4 for each dose of VERU-111 and for paclitaxel. Lung macrometastases visible to the naked eye after H&E staining were only detected in the vehicle group (Fig. 6A). In the 5 mg/kg VERU-111 group, 2 of 8 treated mice did not develop any visible lung metastases, increasing to 4 of 8 mice in the 10 mg/kg VERU-111 treatment group and to 7 of 8 mice in the 12.5 mg/kg VERU-111 group. In comparison, no lung metastases were observed by either H&E staining or IHC in 12.5 mg/kg paclitaxel-treated group (0 of 8 mice developed metastases).

To test if VERU-111 represses the conversion of seeded tumor cells into lethal lung macrometastases, an experimental metastasis (tail vein) model was used. Because mice subjected to experimental metastases typically lose weight as metastases develop, the dose of VERU-111 and paclitaxel was lowered to 10 mg/kg. As expected, metastases were readily detectable in all lungs from the vehicle group, whereas the lungs in VERU-111- and paclitaxel treated groups exhibited considerably fewer metastases, which were also smaller in area (Fig. 6B). Both VERU-111 and paclitaxel were also highly effective in repressing metastasis to the kidney, where no metastases were detected in any mice. In contrast, VERU-111 appeared to be more effective than paclitaxel to repress liver metastases, as fewer lesions were observed (Fig. 6B). Importantly, the body weight (Supplementary Fig. S5A) and the physical activity of mice were normal in VERU-111-treated group. In fact, only the VERU-111 treated mice gained weight over the course of the experiment. As expected, mice in the vehicle treatment group lost weight over time. In the paclitaxel-treated group, mice lost ~10% of their initial body weight, demonstrating the relative toxicity of paclitaxel versus VERU-111. H&E staining also showed that multiple metastases with varying sizes were observed in the lung, liver, and kidney of vehicle treated mice, whereas the metastases in the VERU-111 and paclitaxel-treated mice were overall less frequently observed and were smaller (Supplementary Fig. S5B). Collectively, these results support our conclusions that VERU-111 shows comparable efficacy to paclitaxel in suppressing metastasis of TNBC cells at equivalent doses, but without significant toxicity to mice, and with the distinct advantage of being orally bioavailable.

VERU-111 suppresses the TNBC growth and metastases in a taxane-resistant metastatic mouse model

To determine if VERU-111 is effective in a taxane-resistant TNBC model, we first utilized two primary cell lines derived from well-characterized TNBC patient-derived xenograft (PDX) models to compare colchicine, paclitaxel and VERU-111 efficacy *in vitro*, a treatment-naïve TNBC model (HCI-2-Luc2) and a taxane-resistant TNBC model (HCI-10-Luc2). Because both primary cell lines double slowly, approximately every 3 days (20), the duration of drug treatment was six days. As expected, the HCI-10 cells were more resistant to paclitaxel treatment than HCI-2 cells (grand mean IC_{50} 39.27 ± 5.40 nM vs. 6.20 ± 1.70 nM; determined from n=4 biological replicate experiments) (Fig. 7A and Supplementary Table S2). However, for VERU-111, the IC_{50} concentration in each cell model was nearly equivalent (mean IC_{50} 11.89 ± 2.76 nM versus 10.78 ± 1.20 nM), suggesting that VERU-111 maintained its efficacy to suppress growth of a taxane-resistant TNBC model. Colchicine is included as an assay control, although it is not clinically approved for breast cancer chemotherapy due to high toxicity. The HCI-10 cell line appeared to be refractory to colchicine compared to the HCI-2 cell line (46.08 ± 5.53 nM versus 36.93 ± 10.57 nM), which is likely because relative to HCI-2 cells, HCI-10 cells over-expresses P-gp, which effluxes colchicine (Supplementary Fig. S6A) (17,29). In an independent assay method, using the IncuCyte S3 live cell imager and measuring confluence by phase contrast, similar IC_{50} values and differential responses to treatment with paclitaxel and VERU-111 between the two primary cell lines were also observed (Supplementary Figure S6B). The use of PDX xenograft models derived from patients and primarily passaged in mice are preferred xenograft models due to their conserved similarities to original patient material (19,30,31). We engrafted HCI-10-Luc2 patient-derived tissue fragments into female NSG mice and each recipient entered a treatment cohort when the tumor volume was ~100 mm^3. VERU-111 (10 mg/kg, PO) significantly suppressed xenograft growth over the entire course of the study, whereas there were no significant changes in tumor volume between the vehicle-treated or paclitaxel-treated (10 mg/kg, 1x week, IV) cohorts at any time point (Fig. 7B). It should be noted that the dosing regimen for paclitaxel was changed for the HCI-10 xenograft model since the tumor fragments grow slower *in vivo* than MDA-MB-231 cells. Paclitaxel was provided 10 mg/kg IV 1x/week instead of 12.5 mg/kg IP every other day as in Figure 4 to reduce potential cumulative toxicity due to the extended treatment regimen (~5 weeks longer duration of treatment than used for MDA-MB-231 xenografts) (32). As observed for MDA-MB-231 xenograft model, there was no significant body weight loss during VERU-111 treatment (Fig. 7C). All animals were euthanized after 8 weeks of drug treatment. As expected, tumors in VERU-111 treated mice were significantly smaller than vehicle-treated mice, with reduced mean tumor volume and tumor weight by 73.7% and 72.0%, respectively (Fig. 7D–E). In contrast, paclitaxel treatment slightly increased mean tumor volume and tumor weight relative to the vehicle controls (Fig. 7D–E). Representative tumors of the mean tumor volume from vehicle-treated, paclitaxel-treated and VERU-111-treated mice are shown in Fig. 7F.

A major clinical challenge is to treat established metastases of the stage IV patient. The HCI-10-Luc2 model metastasizes during early tumor outgrowth to the axillary lymph nodes (AxLNs) (20). Therefore, by bio-imaging mice the day prior to drug treatment, after cohorts

were randomized, we were able to identify a subset of mice in each cohort with pre-established AxLN mets prior to drug treatment and then to follow metastatic growth during treatment. There was exponential increase in AxLN metastatic signal measured by total photon flux comparing week 0 on therapy to week 8 on therapy at endpoint between the vehicle and paclitaxel cohorts (100- and 65-fold, respectively, Fig. 7G). In contrast, AxLN metastatic signal increased by only 3.1-fold for the VERU-111 group over the course of the study ($p = 0.006$). Therefore, VERU-111 strongly repressed the growth of pre-established metastases. Furthermore, relative to the vehicle group, paclitaxel had no significant impact on the growth and expansion of pre-established AxLNs metastases. Moreover, analysis of *ex vivo* bio-imaging data collected at the experiment endpoint also revealed that only VERU-111 significantly repressed total photon flux within the AxLNs (Fig. 7H), lungs (Fig. 7I) or leg bones (Fig. 7K). Consistent with our observations in the MDA-MB-231 model, VERU-111 had the most potent effect on repression of liver metastases and, in fact, paclitaxel treatment significantly enhanced liver metastatic burden relative to vehicle controls (Fig. 7I). Representative images of *ex vivo* imaging data are shown in Supplementary Fig. S6C–E.

Discussion

The five-year survival rate of patients diagnosed with metastatic TNBC is less than 30% (33–35). Challenges for TNBC patients are a lack of effective targeted therapies and a more rapid onset of chemoresistance to conventional cytotoxic therapies. Chemotherapy is the primary systemic treatment for patients with TNBC, with the goal of inhibiting cancer cell growth and dissemination (36). Dynamic microtubule organization is one of the most successful targets due to the critical roles of the microtubule network in cell proliferation, particularly cell division (37). FDA-approved drugs, such as paclitaxel, are effective in treating neoadjuvant, adjuvant or metastatic TNBC, but intrinsic or acquired resistance to taxanes is commonly observed. Moreover, paclitaxel needs to be formulated as an albumin-bound formulation or with a vehicle containing Cremophor EL due to poor aqueous solubility and then delivered intravenously by slow infusion (6,38). There are also neurotoxicities associated with taxane agent use, including persistent peripheral neuropathies, which significantly impact the patient's quality of life. As alternatives to paclitaxel, microtubule-targeted agents that bind to the colchicine-binding site of tubulin have attracted recent attention. Several colchicine-binding site inhibitors, including VERU-111, are currently undergoing clinical trials. In contrast, the CBSI combretastatin A-4 phosphate (CA-4) has been evaluated in clinical trials for over a decade and is not yet FDA-approved (14,39).

We previously reported a series of novel 2-aryl-4-benzoyl-imidazoles and derivatives that target the colchicine-binding site with potent cytotoxicity, have improved aqueous solubility and overcome multidrug resistance, including P-gp over-expression (17,40,41). We evaluated VERU-111, the most potent 2-aryl-4-benzoyl-imidazole analog, in the treatment of TNBC, as its anti-proliferative efficacy was not previously defined, using colchicine and paclitaxel as positive controls. We assessed the efficacy of VERU-111 against MDA-MB-231 and MDA-MB-468 TNBC cell lines. VERU-111 showed strong anti-proliferative activity in all these models with an IC_{50} value in the low nanomolar range. In a colony

formation assay, VERU-111 reduced the clonogenic survival of TNBC cells. VERU-111 efficacy was superior to colchicine, although less potent than paclitaxel at the equivalent concentration to repress clonogenic survival.

Most of the microtubule-stabilizing agents enhance microtubule polymerization by targeting taxane-binding site located at the interior surface of the microtubules, while microtubule depolymerizing agents inhibit microtubule polymerization by binding in one of two domains on tubulin (7). To confirm that VERU-111 depolymerizes microtubules, we stained for α-tubulin in TNBC cells treated with VERU-111, which showed that VERU-111-treated cells displayed aberrant microtubule network arrangement and organization, similar to results obtained with colchicine-treated TNBC cells. Therefore, VERU-111 is a novel microtubule-depolymerizing agent. Due to the pivotal role of asymmetric regulation of microtubule dynamics and stability played in cell migration and invasion, we then investigated the effect of VERU-111 using cell migration and invasion assays (42,43). Our results showed that VERU-111 inhibited TNBC cell motility and invasion potently.

Several anti-mitotic agents have been reported to target microtubules, disrupt microtubule dynamics, induce cell cycle arrest and cause eventual cell death (44,45). We found that VERU-111 arrested MDA-MB-231 cells at the G2/M checkpoint in a concentration-dependent manner. The effects of colchicine, paclitaxel and VERU-111 were similar in MDA-MB-231 cells, with accumulated cells at the G2/M checkpoint; VERU-111 also induced cells into the M phase in a concentration-dependent manner. However, VERU-111 or colchicine primarily induced a G2 phase arrest in MDA-MB-468 cells, whereas paclitaxel arrested cells in both the G2 and M phase. One reason for this result may be that MDA-MB-231 cells are a “type A” cell line that displays prominent mitotic arrest, whereas the MDA-MB-468 cell line is a “type B” cell line, displaying less prominent mitotic arrest, but possessing significant mitotic arrest at higher concentrations of microtubule-targeting agents (46). It is widely believed that anti-mitotic agents cause apoptosis along with cell cycle arrest (47,48). Cleaved-caspase-3 is an effector caspase involved in both intrinsic and extrinsic apoptosis pathways; it can cleave its downstream target PARP, which conducts DNA damage repair (49,50). VERU-111 induced cell apoptosis in a time-and concentration-dependent manner, and it promoted the cleavage of caspase-3 and PARP in MDA-MB-231 and MDA-MB-468 cells. Together, these results indicate that VERU-111 induces cell cycle arrest and ultimately apoptosis in TNBC cells.

The chemotherapeutic strategies for treating TNBC primarily include DNA-damaging agents, anti-mitotic agents and targeted anti-angiogenic therapy. For example, the combination uses of carboplatin, paclitaxel and bevacizumab, respectively, is recommended as a first-line or second-line therapy for TNBC treatment (51–53). However, novel chemotherapies are required to improve the survival rates for TNBC due to taxane-induced dose-limiting neurotoxicities or cardiotoxicities and acquired resistance to taxanes (54). We evaluated the antitumor effect of orally delivered VERU-111 versus paclitaxel (provided IP or IV) in two orthotopic, highly metastatic TNBC models to determine if VERU-111 is an efficacious novel anti-tubulin inhibitor to treat TNBC. For the MDA-MB-231 xenograft model, for which cells were not previously exposed to taxanes, VERU-111 inhibited TNBC tumor growth in a dose-dependent manner without reducing body weight, and with

equivalent efficacy to paclitaxel to reduce tumor volume/wet weight. Both drugs were observed to increase tumor necrosis, to decrease cancer cell proliferation, to reduce angiogenesis and to cause apoptotic cell death via increased the expression of cleaved-caspase-3 and cleaved-PARP.

TNBC frequently progresses to stage IV, metastatic disease, the leading cause of breast cancer-associated mortality (55). In the MDA-MB-231 model, either paclitaxel or VERU-111 inhibited the formation of lung metastasis from the mammary pad, reducing the total number and size of metastases that had completed the entire metastatic cascade. One limitation in this experiment is that the tumors were not equal sizes at the time of euthanasia and lung harvest (both paclitaxel- and VERU-111-treated tumors were smaller than vehicle-treated tumors). Therefore, to bypass primary tumor growth, we supplemented these results by a tail vein assay in which mice were treated with either VERU-111 or paclitaxel 24 h after tumor cell injection. Fewer metastases were observed in lungs, livers and kidneys by H&E or IHC following VERU-111 or paclitaxel treatment. Although both drugs appeared equally effective to repress lung and kidney metastasis, VERU-111 appeared to be more effective than paclitaxel in reducing liver metastasis.

Finally, we have shown *in vitro* that VERU-111 is efficacious at similar nM concentrations *in vitro* for both a taxane-resistant patient-derived primary cell line (HCI-10-Luc2) and a treatment-naïve patient-derived primary cell line (HCI-2-Luc2). In contrast, the IC_{50} concentration of paclitaxel required to inhibit growth of HCI-10 cells was between 6.33 and 8.5-fold higher than for HCI-2 cells, depending on the method used to calculate IC_{50} values. These data provide rationale that VERU-111 likely bypasses taxane resistance in breast cancer, as we have previously shown for VERU-111 in prostate cancer models (18). VERU-111 efficacy was then tested *in vivo* using the luciferase-labeled HCI-10 taxane-resistant model. VERU-111 therapy was highly effective in blocking primary tumor growth, whereas paclitaxel treatment was completely ineffective relative to vehicle-treated controls at all time points. In addition, VERU-111 treatment significantly reduced outgrowth of pre-established AxLN metastases over the course of drug treatment and the endpoint metastatic burden for AxLNs, lung, and bone while blocking liver metastasis. Collectively, these data strongly suggest that VERU-111 may also be an effective second line therapy for TNBC patients who progress on taxanes (i.e. develop taxane resistance).

In summary, we have shown *in vivo* in two aggressive TNBC xenograft models that a novel microtubule-targeting agent to the colchicine-binding site, VERU-111, which is orally bioavailable and well-tolerated, displays potent anti-breast cancer activity, including anti-metastatic potential. VERU-111 has been previously reported to inhibit tubulin polymerization and to effectively overcome P-gp-mediated multidrug resistance, which frequently develops in patients treated with conventional taxanes (17). The distinct advantages of VERU-111 therapy include equivalent efficacy as paclitaxel *in vitro* and in treatment-naïve TNBC cell line models, and the ability to effectively treat taxane-resistant disease *in vivo*. Moreover, compared to taxanes, VERU-111 analogs do not induce peripheral neuropathy in mice and dogs (56), addressing a currently unmet clinical challenge impacting patient quality of life. A Phase 1/2 clinical trial of VERU-111 has begun for patients with advanced prostate cancer, including patients who have already failed taxane-

based therapies. Our results suggest that clinical trials for stage IV metastatic breast cancer patients, including patients diagnosed with TNBC, are also supported by strong preclinical data.

Supplementary Material

Refer to Web version on PubMed Central for supplementary material.

Acknowledgements

We thank Dr. Louisa Balazs and the UTHSC Research Histology Core (RHC) for assistance in quantifying the necrotic percentage of representative tumor tissues and Drs. Deidre Daria and Tony Marion of the UTHSC Flow Cytometry and Cell Sorting (FCCS) core for assistance with cell cycle analysis using FlowJo. We thank Dr. Radika Sekhri and the Department of Pathology for generously scanning all stained slides. We thank Dr. Alana Welm at the Huntsman Cancer Institute (HCI) for providing the original PDX models and for performing whole-genome expression analysis of the Luc2-labeled PDX derivatives to verify their origin.

Financial support: This work was supported by the NIH grants 1R01CA193609 (W. Li), R01CA148706 (W. Li and D. D. Miller), R01CA138488 (T. Seagroves), and the 2018 West Cancer Center Research Awards to W. Li and to T. Seagroves. The contents are solely the responsibility of the authors and do not necessarily represent the official views of the NIH.

Conflict of interest statement

Dr. Wei Li is currently serving as a consultant to Veru Inc., who licensed the patents covering Veru-111 reported in this manuscript for commercial development. Veru Inc. did not provide any financial support or have any influence on research design, data collections, data analyses, or the writing of this manuscript.

Abbreviations

ABC	ATP-binding cassette
AxLN	Axillary lymph nodes
CBSIs	Colchicine binding site inhibitors
H&E	Hematoxylin / eosin
HER2	Human epidermal growth factor receptor 2
IHC	Immunohistochemistry
NSG	NOD scid gamma
PARP	Poly (ADP-ribose) polymerase
P-gp	P-glycoprotein
PDX	patient-derived xenograft
TNBC	Triple-negative breast cancer

References

1. Siegel RL, Miller KD, Jemal A. Cancer statistics, 2018. CA Cancer J Clin 2018;68(1):7–30 doi 10.3322/caac.21442. [PubMed: 29313949]

2. Yeh J, Chun J, Schwartz S, Wang A, Kern E, Guth AA, et al. Clinical Characteristics in Patients with Triple Negative Breast Cancer. Int J Breast Cancer 2017;2017:1796145 doi 10.1155/2017/1796145. [PubMed: 28912973]

3. Al-Mahmood S, Sapiezynski J, Garbuzenko OB, Minko T. Metastatic and triple-negative breast cancer: challenges and treatment options. Drug Deliv Transl Res 2018 doi 10.1007/s13346-018-0551-3.

4. Kennecke H, Yerushalmi R, Woods R, Cheang MC, Voduc D, Speers CH, et al. Metastatic behavior of breast cancer subtypes. J Clin Oncol 2010;28(20):3271–7 doi 10.1200/JCO.2009.25.9820. [PubMed: 20498394]

5. Lebert JM, Lester R, Powell E, Seal M, McCarthy J. Advances in the systemic treatment of triple-negative breast cancer. Curr Oncol 2018;25(Suppl 1):S142–S50 doi 10.3747/co.25.3954. [PubMed: 29910657]

6. Mustacchi G, De Laurentiis M. The role of taxanes in triple-negative breast cancer: literature review. Drug Des Devel Ther 2015;9:4303–18 doi 10.2147/DDDT.S86105.

7. Dumontet C, Jordan MA. Microtubule-binding agents: a dynamic field of cancer therapeutics. Nat Rev Drug Discov 2010;9(10):790–803 doi 10.1038/nrd3253. [PubMed: 20885410]

8. Lopus M, Naik PK. Taking aim at a dynamic target: Noscapinoids as microtubule-targeted cancer therapeutics. Pharmacol Rep 2015;67(1):56–62 doi 10.1016/j.pharep.2014.09.003. [PubMed: 25560576]

9. Nakagawa-Goto K, Oda A, Hamel E, Ohkoshi E, Lee KH, Goto M. Development of a novel class of tubulin inhibitor from desmosdumotin B with a hydroxylated bicyclic B-ring. J Med Chem 2015;58(5):2378–89 doi 10.1021/jm501859j. [PubMed: 25695315]

10. Wu X, Wang Q, Li W. Recent Advances in Heterocyclic Tubulin Inhibitors Targeting the Colchicine Binding Site. Anticancer Agents Med Chem 2016;16(10):1325–38. [PubMed: 26899186]

11. Perez EA. Impact, mechanisms, and novel chemotherapy strategies for overcoming resistance to anthracyclines and taxanes in metastatic breast cancer. Breast Cancer Res Treat 2009;114(2):195–201 doi 10.1007/s10549-008-0005-6. [PubMed: 18443902]

12. Perez EA. Microtubule inhibitors: Differentiating tubulin-inhibiting agents based on mechanisms of action, clinical activity, and resistance. Mol Cancer Ther 2009;8(8):2086–95 doi 10.1158/1535-7163.MCT-09-0366. [PubMed: 19671735]

13. Wang Z, Chen J, Wang J, Ahn S, Li CM, Lu Y, et al. Novel tubulin polymerization inhibitors overcome multidrug resistance and reduce melanoma lung metastasis. Pharm Res 2012;29(11):3040–52 doi 10.1007/s11095-012-0726-4. [PubMed: 22410804]

14. Li L, Jiang S, Li X, Liu Y, Su J, Chen J. Recent advances in trimethoxyphenyl (TMP) based tubulin inhibitors targeting the colchicine binding site. Eur J Med Chem 2018;151:482–94 doi 10.1016/j.ejmech.2018.04.011. [PubMed: 29649743]

15. Subbiah IM, Lenihan DJ, Tsimberidou AM. Cardiovascular toxicity profiles of vascular-disrupting agents. Oncologist 2011;16(8):1120–30 doi 10.1634/theoncologist.2010-0432. [PubMed: 21742963]

16. Tsimberidou AM, Akerley W, Schabel MC, Hong DS, Uehara C, Chhabra A, et al. Phase I clinical trial of MPC-6827 (Azixa), a microtubule destabilizing agent, in patients with advanced cancer. Mol Cancer Ther 2010;9(12):3410–9 doi 10.1158/1535-7163.MCT-10-0516. [PubMed: 21159616]

17. Chen J, Ahn S, Wang J, Lu Y, Dalton JT, Miller DD, et al. Discovery of novel 2-aryl-4-benzoyl-imidazole (ABI-III) analogues targeting tubulin polymerization as antiproliferative agents. J Med Chem 2012;55(16):7285–9 doi 10.1021/jm300564b. [PubMed: 22783954]

18. Li CM, Lu Y, Chen J, Costello TA, Narayanan R, Dalton MN, et al. Orally bioavailable tubulin antagonists for paclitaxel-refractory cancer. Pharm Res 2012;29(11):3053–63 doi 10.1007/s11095-012-0814-5. [PubMed: 22760659]

19. DeRose YS, Gligorich KM, Wang G, Georgelas A, Bowman P, Courdy SJ, et al. Patient-derived models of human breast cancer: protocols for in vitro and in vivo applications in tumor biology and translational medicine. Curr Protoc Pharmacol 2013;Chapter 14:Unit14 23 doi 10.1002/0471141755.ph1423s60.

20. El Ayachi I, Fatima I, Wend P, Alva-Ornelas JA, Runke S, Kuenzinger WL, et al. The WNT10B Network Is Associated with Survival and Metastases in Chemoresistant Triple-Negative Breast Cancer. Cancer Res 2019;79(5):982–93 doi 10.1158/0008-5472.CAN-18-1069. [PubMed: 30563890]
21. Wang Q, Arnst KE, Wang Y, Kumar G, Ma D, Chen H, et al. Structural Modification of the 3,4,5-Trimethoxyphenyl Moiety in the Tubulin Inhibitor VERU-111 Leads to Improved Antiproliferative Activities. J Med Chem 2018 doi 10.1021/acs.jmedchem.8b00827.
22. Xiao M, Wang J, Lin Z, Lu Y, Li Z, White SW, et al. Design, Synthesis and Structure-Activity Relationship Studies of Novel Survivin Inhibitors with Potent Anti-Proliferative Properties. PLoS One 2015;10(6):e0129807 doi 10.1371/journal.pone.0129807. [PubMed: 26070194]
23. Fan M, Krutilina R, Sun J, Sethuraman A, Yang CH, Wu ZH, et al. Comprehensive analysis of microRNA (miRNA) targets in breast cancer cells. J Biol Chem 2013;288(38):27480–93 doi 10.1074/jbc.M113.491803. [PubMed: 23921383]
24. Mollinedo F, Gajate C. Microtubules, microtubule-interfering agents and apoptosis. Apoptosis 2003;8(5):413–50. [PubMed: 12975575]
25. Kulshrestha A, Katara GK, Ibrahim SA, Patil R, Patil SA, Beaman KD. Microtubule inhibitor, SP-6–27 inhibits angiogenesis and induces apoptosis in ovarian cancer cells. Oncotarget 2017;8(40):67017–28 doi 10.18632/oncotarget.17549. [PubMed: 28978013]
26. Xu P, Cai X, Zhang W, Li Y, Qiu P, Lu D, et al. Flavonoids of Rosa roxburghii Tratt exhibit radioprotection and anti-apoptosis properties via the Bcl-2(Ca(2+))/Caspase-3/PARP-1 pathway. Apoptosis 2016;21(10):1125–43 doi 10.1007/s10495-016-1270-1. [PubMed: 27401922]
27. Wang W, Deng Z, Feng Y, Liao F, Zhou F, Feng S, et al. PM2.5 induced apoptosis in endothelial cell through the activation of the p53-bax-caspase pathway. Chemosphere 2017;177:135–43 doi 10.1016/j.chemosphere.2017.02.144. [PubMed: 28284960]
28. Bocci G, Di Paolo A, Danesi R. The pharmacological bases of the antiangiogenic activity of paclitaxel. Angiogenesis 2013;16(3):481–92 doi 10.1007/s10456-013-9334-0. [PubMed: 23389639]
29. Taub ME, Podila L, Ely D, Almeida I. Functional assessment of multiple P-glycoprotein (P-gp) probe substrates: influence of cell line and modulator concentration on P-gp activity. Drug Metab Dispos 2005;33(11):1679–87 doi 10.1124/dmd.105.005421. [PubMed: 16093365]
30. Tentler JJ, Tan AC, Weekes CD, Jimeno A, Leong S, Pitts TM, et al. Patient-derived tumour xenografts as models for oncology drug development. Nat Rev Clin Oncol 2012;9(6):338–50 doi 10.1038/nrclinonc.2012.61. [PubMed: 22508028]
31. Siolas D, Hannon GJ. Patient-derived tumor xenografts: transforming clinical samples into mouse models. Cancer Res 2013;73(17):5315–9 doi 10.1158/0008-5472.CAN-13-1069. [PubMed: 23733750]
32. Liapis V, Zinonos I, Labrinidis A, Hay S, Ponomarev V, Panagopoulos V, et al. Anticancer efficacy of the hypoxia-activated prodrug evofosfamide (TH-302) in osteolytic breast cancer murine models. Cancer Med 2016;5(3):534–45 doi 10.1002/cam4.599. [PubMed: 26749324]
33. Blows FM, Driver KE, Schmidt MK, Broeks A, van Leeuwen FE, Wesseling J, et al. Subtyping of breast cancer by immunohistochemistry to investigate a relationship between subtype and short and long term survival: a collaborative analysis of data for 10,159 cases from 12 studies. PLoS Med 2010;7(5):e1000279 doi 10.1371/journal.pmed.1000279. [PubMed: 20520800]
34. Oba T, Ito KI. Combination of two anti-tubulin agents, eribulin and paclitaxel, enhances anti-tumor effects on triple-negative breast cancer through mesenchymal-epithelial transition. Oncotarget 2018;9(33):22986–3002 doi 10.18632/oncotarget.25184. [PubMed: 29796167]
35. Tate CR, Rhodes LV, Segar HC, Driver JL, Pounder FN, Burow ME, et al. Targeting triple-negative breast cancer cells with the histone deacetylase inhibitor panobinostat. Breast Cancer Res 2012;14(3):R79 doi 10.1186/bcr3192. [PubMed: 22613095]
36. Montagna E, Maisonneuve P, Rotmensz N, Cancello G, Iorfida M, Balduzzi A, et al. Heterogeneity of triple-negative breast cancer: histologic subtyping to inform the outcome. Clin Breast Cancer 2013;13(1):31–9 doi 10.1016/j.clbc.2012.09.002. [PubMed: 23098574]

37. Field JJ, Kanakkanthara A, Miller JH. Microtubule-targeting agents are clinically successful due to both mitotic and interphase impairment of microtubule function. Bioorg Med Chem 2014;22(18): 5050–9 doi 10.1016/j.bmc.2014.02.035. [PubMed: 24650703]
38. Stage TB, Bergmann TK, Kroetz DL. Clinical Pharmacokinetics of Paclitaxel Monotherapy: An Updated Literature Review. Clin Pharmacokinet 2018;57(1):7–19 doi 10.1007/s40262-017-0563-z. [PubMed: 28612269]
39. Garon EB, Neidhart JD, Gabrail NY, de Oliveira MR, Balkissoon J, Kabbinavar F. A randomized Phase II trial of the tumor vascular disrupting agent CA4P (fosbretabulin tromethamine) with carboplatin, paclitaxel, and bevacizumab in advanced nonsquamous non-small-cell lung cancer. Onco Targets Ther 2016;9:7275–83 doi 10.2147/OTT.S109186. [PubMed: 27942221]
40. Chen J, Wang Z, Li CM, Lu Y, Vaddady PK, Meibohm B, et al. Discovery of novel 2-aryl-4-benzoyl-imidazoles targeting the colchicines binding site in tubulin as potential anticancer agents. J Med Chem 2010;53(20):7414–27 doi 10.1021/jm100884b. [PubMed: 20919720]
41. Chen J, Li CM, Wang J, Ahn S, Wang Z, Lu Y, et al. Synthesis and antiproliferative activity of novel 2-aryl-4-benzoyl-imidazole derivatives targeting tubulin polymerization. Bioorg Med Chem 2011;19(16):4782–95 doi 10.1016/j.bmc.2011.06.084. [PubMed: 21775150]
42. Etienne-Manneville S. Microtubules in cell migration. Annu Rev Cell Dev Biol 2013;29:471–99 doi 10.1146/annurev-cellbio-101011-155711. [PubMed: 23875648]
43. Lupo B, Vialard J, Sassi F, Angibaud P, Puliafito A, Pupo E, et al. Tankyrase inhibition impairs directional migration and invasion of lung cancer cells by affecting microtubule dynamics and polarity signals. BMC Biol 2016;14:5 doi 10.1186/s12915-016-0226-9. [PubMed: 26787475]
44. Ganansia-Leymarie V, Bischoff P, Bergerat JP, Holl V. Signal transduction pathways of taxanes-induced apoptosis. Curr Med Chem Anticancer Agents 2003;3(4):291–306. [PubMed: 12769774]
45. Choi JY, Hong WG, Cho JH, Kim EM, Kim J, Jung CH, et al. Podophyllotoxin acetate triggers anticancer effects against non-small cell lung cancer cells by promoting cell death via cell cycle arrest, ER stress and autophagy. Int J Oncol 2015;47(4):1257–65 doi 10.3892/ijo.2015.3123. [PubMed: 26314270]
46. Blajeski AL, Phan VA, Kottke TJ, Kaufmann SH. G(1) and G(2) cell-cycle arrest following microtubule depolymerization in human breast cancer cells. J Clin Invest 2002;110(1):91–9 doi 10.1172/JCI13275. [PubMed: 12093892]
47. Bates D, Feris EJ, Danilov AV, Eastman A. Rapid induction of apoptosis in chronic lymphocytic leukemia cells by the microtubule disrupting agent BNC105. Cancer Biol Ther 2016;17(3):291–9 doi 10.1080/15384047.2016.1139245. [PubMed: 26891146]
48. Qi C, Wang X, Shen Z, Chen S, Yu H, Williams N, et al. Anti-mitotic chemotherapeutics promote apoptosis through TL1A-activated death receptor 3 in cancer cells. Cell Res 2018;28(5):544–55 doi 10.1038/s41422-018-0018-6. [PubMed: 29497138]
49. Swindall AF, Stanley JA, Yang ES. PARP-1: Friend or Foe of DNA Damage and Repair in Tumorigenesis? Cancers (Basel) 2013;5(3):943–58 doi 10.3390/cancers5030943. [PubMed: 24202328]
50. Harrington HA, Ho KL, Ghosh S, Tung KC. Construction and analysis of a modular model of caspase activation in apoptosis. Theor Biol Med Model 2008;5:26 doi 10.1186/1742-4682-5-26. [PubMed: 19077196]
51. Wahba HA, El-Hadaad HA. Current approaches in treatment of triple-negative breast cancer. Cancer Biol Med 2015;12(2):106–16 doi 10.7497/j.issn.2095-3941.2015.0030. [PubMed: 26175926]
52. Guarneri V, Dieci MV, Bisagni G, Boni C, Cagossi K, Puglisi F, et al. Preoperative carboplatin-paclitaxel-bevacizumab in triple-negative breast cancer: final results of the phase II Ca.Pa.Be study. Ann Surg Oncol 2015;22(9):2881–7 doi 10.1245/s10434-015-4371-0. [PubMed: 25572687]
53. Saloustros E, Nikolaou M, Kalbakis K, Polyzos A, Christofillakis C, Kentepozidis N, et al. Weekly Paclitaxel and Carboplatin Plus Bevacizumab as First-Line Treatment of Metastatic Triple-Negative Breast Cancer. A Multicenter Phase II Trial by the Hellenic Oncology Research Group. Clin Breast Cancer 2018;18(1):88–94 doi 10.1016/j.clbc.2017.10.013. [PubMed: 29153775]

54. Twelves C, Jove M, Gombos A, Awada A. Cytotoxic chemotherapy: Still the mainstay of clinical practice for all subtypes metastatic breast cancer. Crit Rev Oncol Hematol 2016;100:74–87 doi 10.1016/j.critrevonc.2016.01.021. [PubMed: 26857987]

55. Mayer IA, Abramson VG, Lehmann BD, Pietenpol JA. New strategies for triple-negative breast cancer--deciphering the heterogeneity. Clin Cancer Res 2014;20(4):782–90 doi 10.1158/1078-0432.CCR-13-0583. [PubMed: 24536073]

56. Ahn S, Duke CB 3rd, Barrett CM, Hwang DJ, Li CM, Miller DD, et al. I-387, a novel antimitotic indole, displays a potent in vitro and in vivo antitumor activity with less neurotoxicity. Mol Cancer Ther 2010;9(11):2859–68 doi 10.1158/1535-7163.MCT-10-0399. [PubMed: 20829196]

Significance

Results presented in this study demonstrate the efficacy of VERU-111 *in vivo* and provide strong rationale for future development of VERU-111 as an effective treatment for metastatic breast cancer.

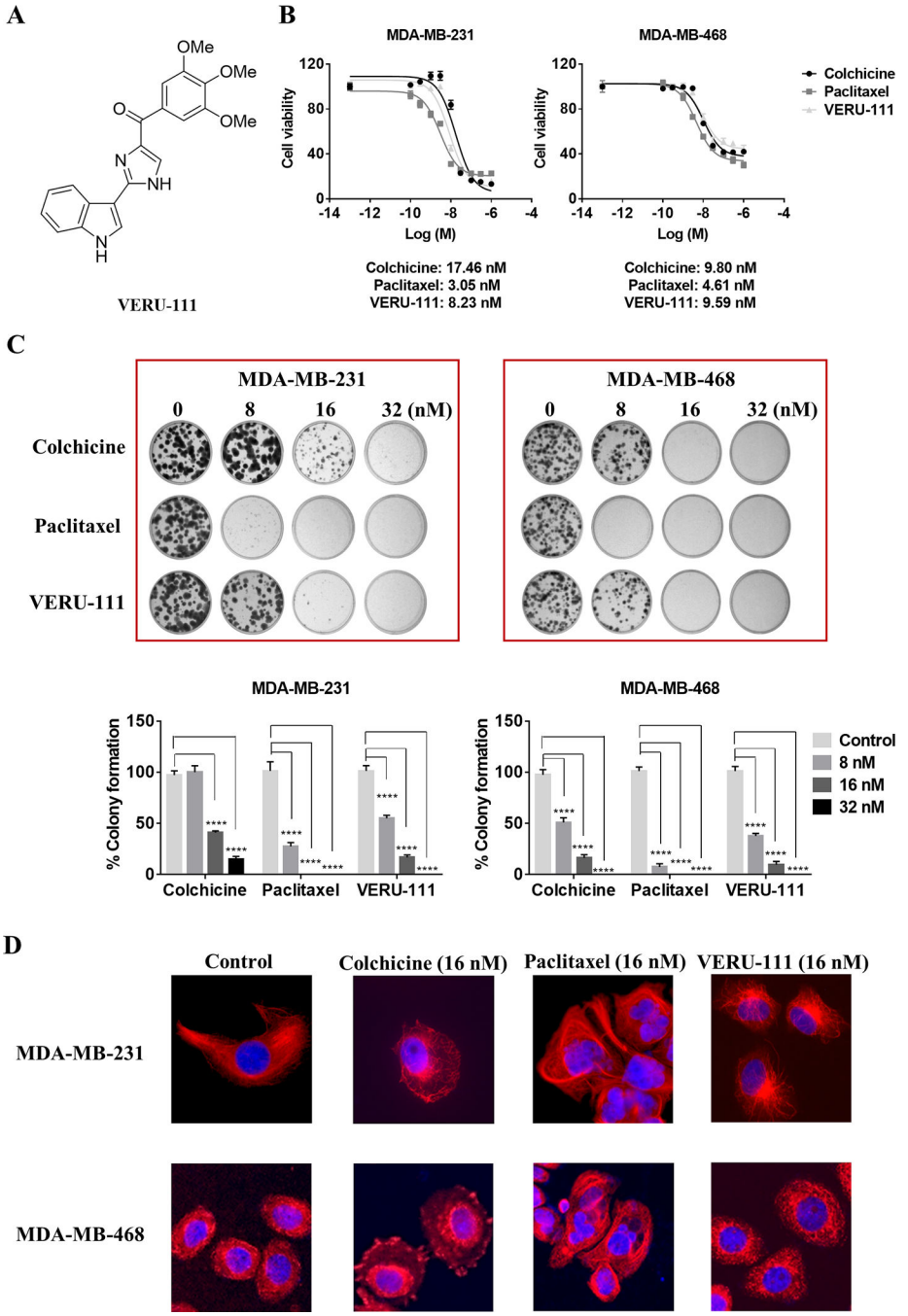

Figure 1.

Efficacy of VERU-111 versus paclitaxel in two TNBC cell lines, MDA-MB-231 and MDA-MB-468. (A) Chemical structure of VERU-111. (B) The anti-proliferative effect of VERU-111 relative to colchicine and paclitaxel controls determined by MTS assay after 72 h (response curves representative of three independent biological replicates are shown; also refer to Supplementary Table S1). (C) Representative pictures of a colony formation assay using MDA-MB-231 (left panel) and MDA-MB-468 (right panel) cells treated with colchicine, paclitaxel and VERU-111 at increasing concentrations (8, 16 or 32 nM) for 7

days and 14 days, respectively. Quantification of colony formation area is expressed as the grand mean ± SEM compared to vehicle control (set to 100%) of three biological replicate experiments. (D) Representative immunofluorescence anti-tubulin staining images of the microtubule network in MDA-MB-231 (top panel) and MDA-MB-468 (lower panel) cells treated with vehicle (Control), colchicine (16 nM), paclitaxel (16 nM) and VERU-111 (16 nM) for 16 h. Images were obtained at ×20 magnification.

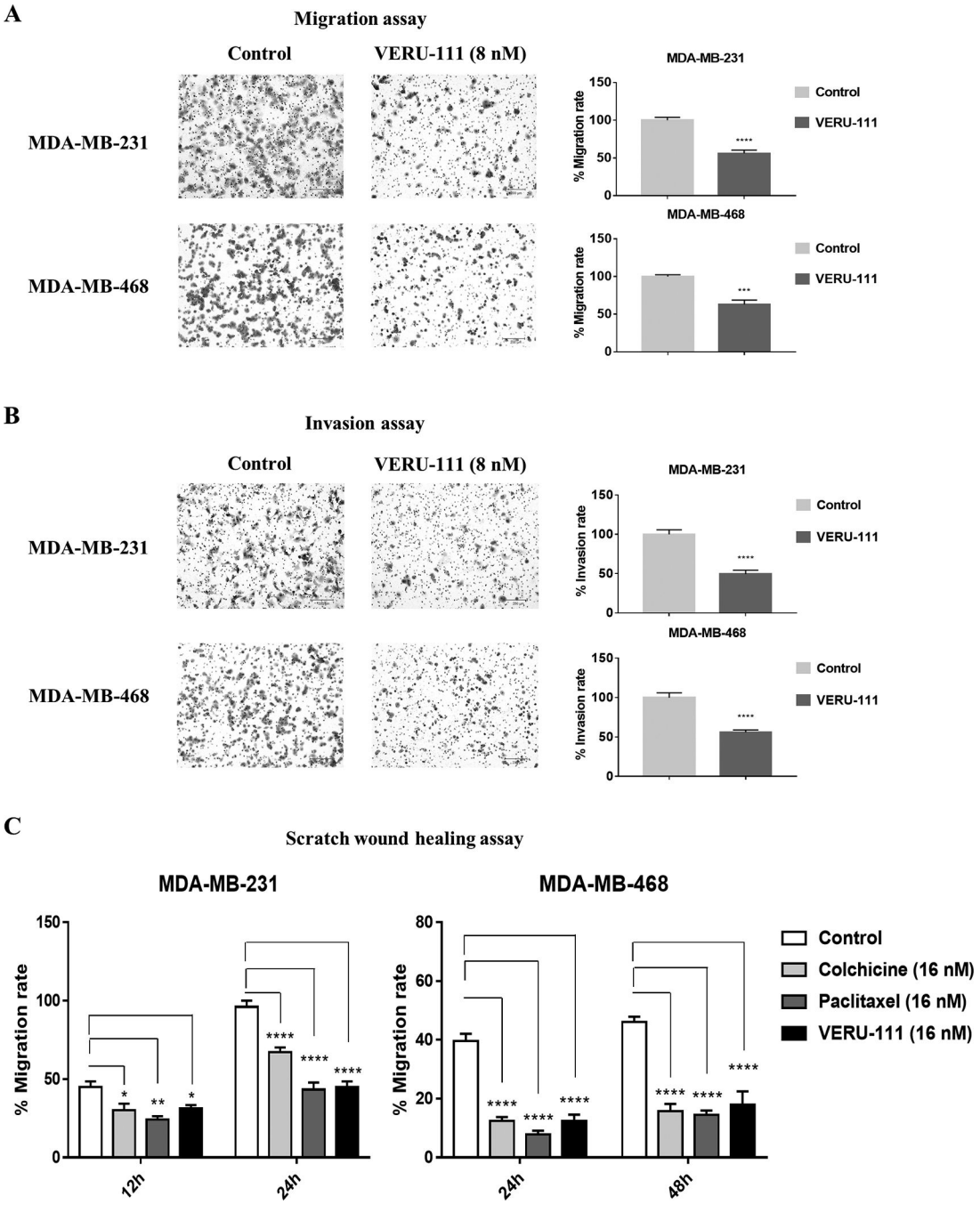

Figure 2.

VERU-111 represses TNBC cell migration and invasion. Directed migration (A) or invasion (B) of MDA-MB-231 (upper panel) and MDA-MB-468 (lower panel) cells was determined using a transwell 24-well plate assay following treatment with VERU-111 (8 nM) for 24 h and 48 h, respectively. (C) The effect of VERU-111 on MDA-MB-231 (left panel) and MDA-MB-468 (right panel) on wound healing was determined by the scratch assay after treatment for 24 h and 48 h, respectively. Migration rates of cells treated with VERU-111, colchicine and paclitaxel (each 16 nM) were determined by the percentage of wound closure

relative to cells in the Control group. All data (A-C) are presented as the grand mean ± SEM of three independent experiments, with *p*-values determined relative to the Control group (normalized to 100%). All images are shown with a scale bar = 200 μm.

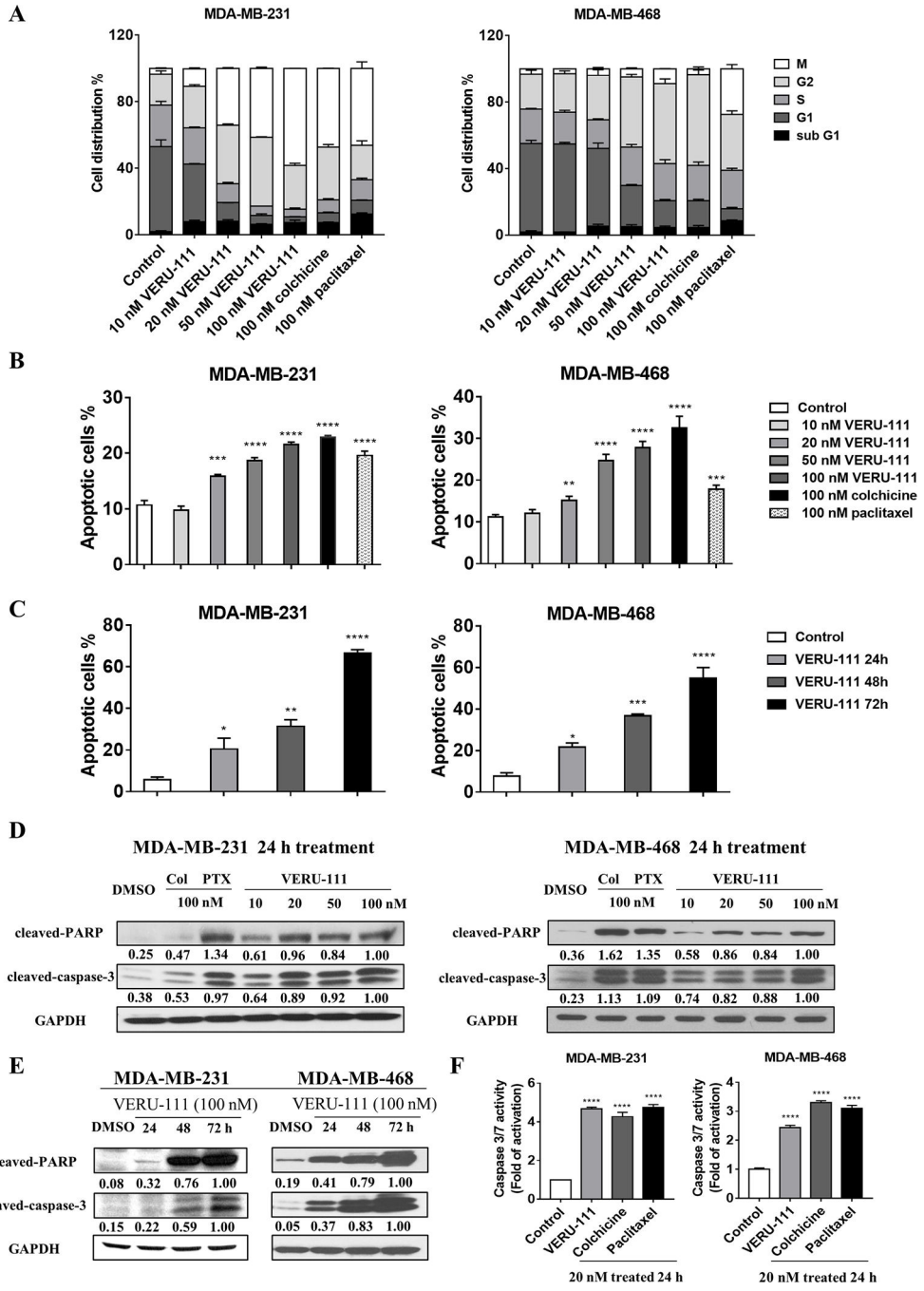

Figure 3.

VERU-111 induces G2/M cell cycle arrest and apoptosis in TNBC cells. (A) Cell cycle distribution was determined by flow cytometry after staining of MDA-MB-231 cells (left panel) and MDA-MB-468 cells (right panel) with phospho-Histone H3 (Ser10) and propidium iodide post-treatment with 100 nM colchicine or 100 nM paclitaxel as controls, or VERU-111 at concentrations of 10, 20, 50 and 100 nM for 24 h. The percentage of cells in each phase of the cell cycle is shown as the grand mean ± SEM calculated from three independent experiments. (B) Apoptosis was compared after treatment with the same drugs

by Annexin-V/PI co-staining and flow cytometry analysis expressed as the grand mean of the apoptotic cells (%) ± SEM calculated from three independent experiments, as compared to Control. (C) Flow cytometry analysis of apoptotic cells detected by Annexin-V/PI staining in MDA-MB-231 (left panel) and MDA-MB-468 cells (right panel) treated with vehicle, or VERU-111 at 100 nM for 24, 48, or 72 h, expressed as the grand mean of the apoptotic cells (%)± SEM of three independent experiments, as compared to Control. (D) Cleaved-caspase-3 and PARP cleavage were determined by western blotting after treatments as in A. GAPDH was used as a loading control. Signal intensity was evaluated by ImageJ densitometry, with 100 nM VERU-111 treatment set to 1.00. (E) Cleaved-caspase-3 and PARP cleavage by western blotting following VERU-111 treatment (100 nM) for 24, 48 and 72 h. Signal intensity was evaluated by ImageJ densitometry, with 100 nM VERU-111 treatment at 72h set to 1.00. (F) Caspase 3/7 activity following treatment with 20 nM of each drug for 24h in MDA-MB-231 (left panel) and MDA-MB-468 (right panel) cells. Bar graphs represent the grand mean of the fold change of caspase 3/7 activity± SEM of three independent experiments as compared to Control.

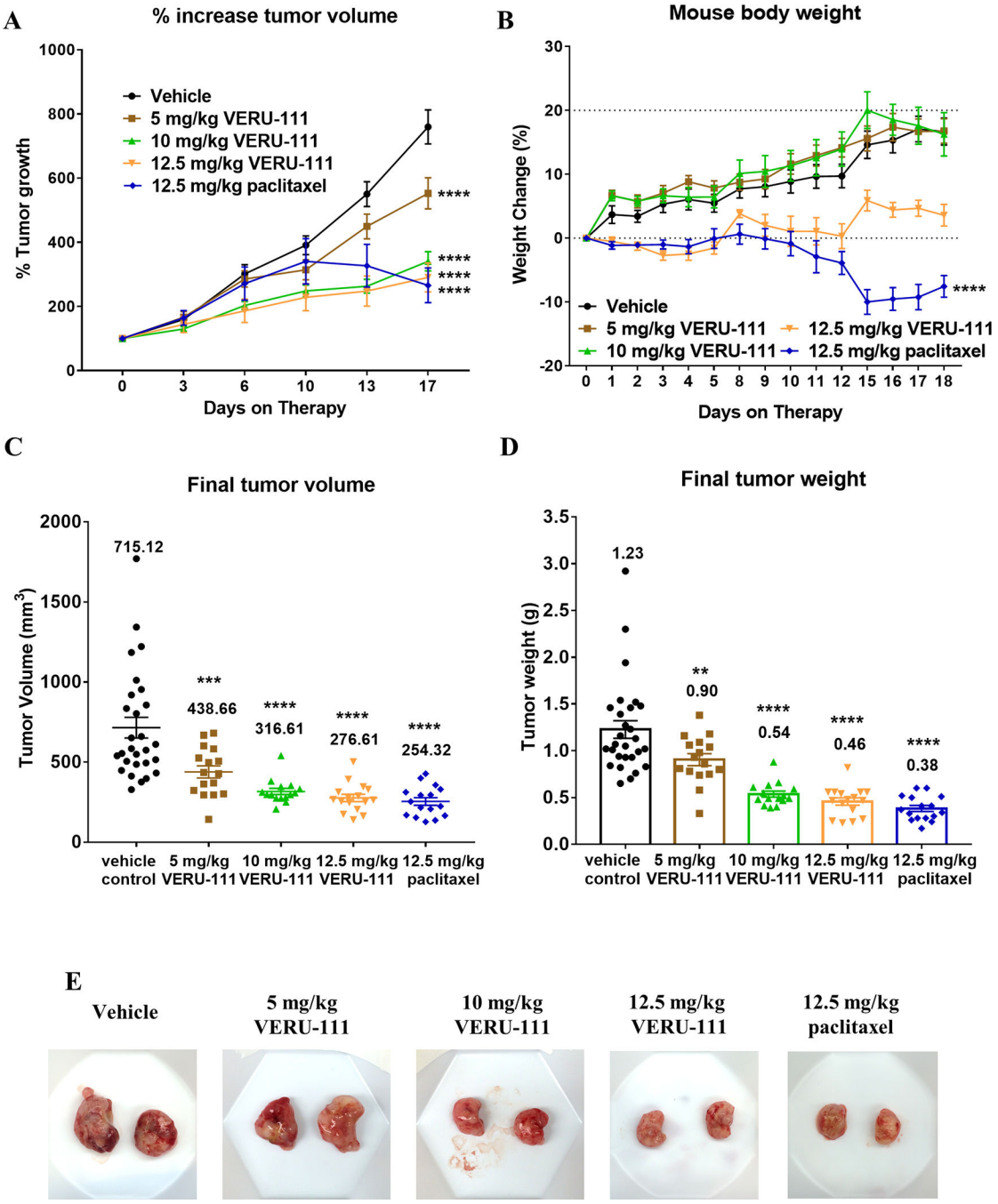

Figure 4.

Antitumor effect of VERU-111 in orthotopic MDA-MB-231 xenografts. For all comparisons, one-way ANOVA was performed followed by Dunnett's multiple comparisons testing and all *p*-values are relative to the vehicle control group at experimental endpoint. (A) The mean percent increase ± SEM in tumor volume relative to initial tumor volume when drug treatment began (tumors ~100 mm^3) following dosing with 5, 10, or 12.5 mg/kg VERU-111 (5 times/week, PO) or 12.5 mg/kg paclitaxel (every other day, IP). (B) Mean percent change in mouse body weight ± SEM relative to body weight at the time of initiating

drug treatment. Dashed lines indicate weight relative to the baseline (y axis = 0) and 20% weight gain. (A-B) Time is expressed as days post-injection of MDA-MB-231 cells to the mammary fat pad. (C-D) Scatter plots of final tumor volume ± SEM of excised tumors measured *ex vivo* with calipers (C) and final tumor weight wet (D); the mean is indicated above each treatment group. (E) Images representative of tumors for each cohort's mean final tumor volume and wet weight.

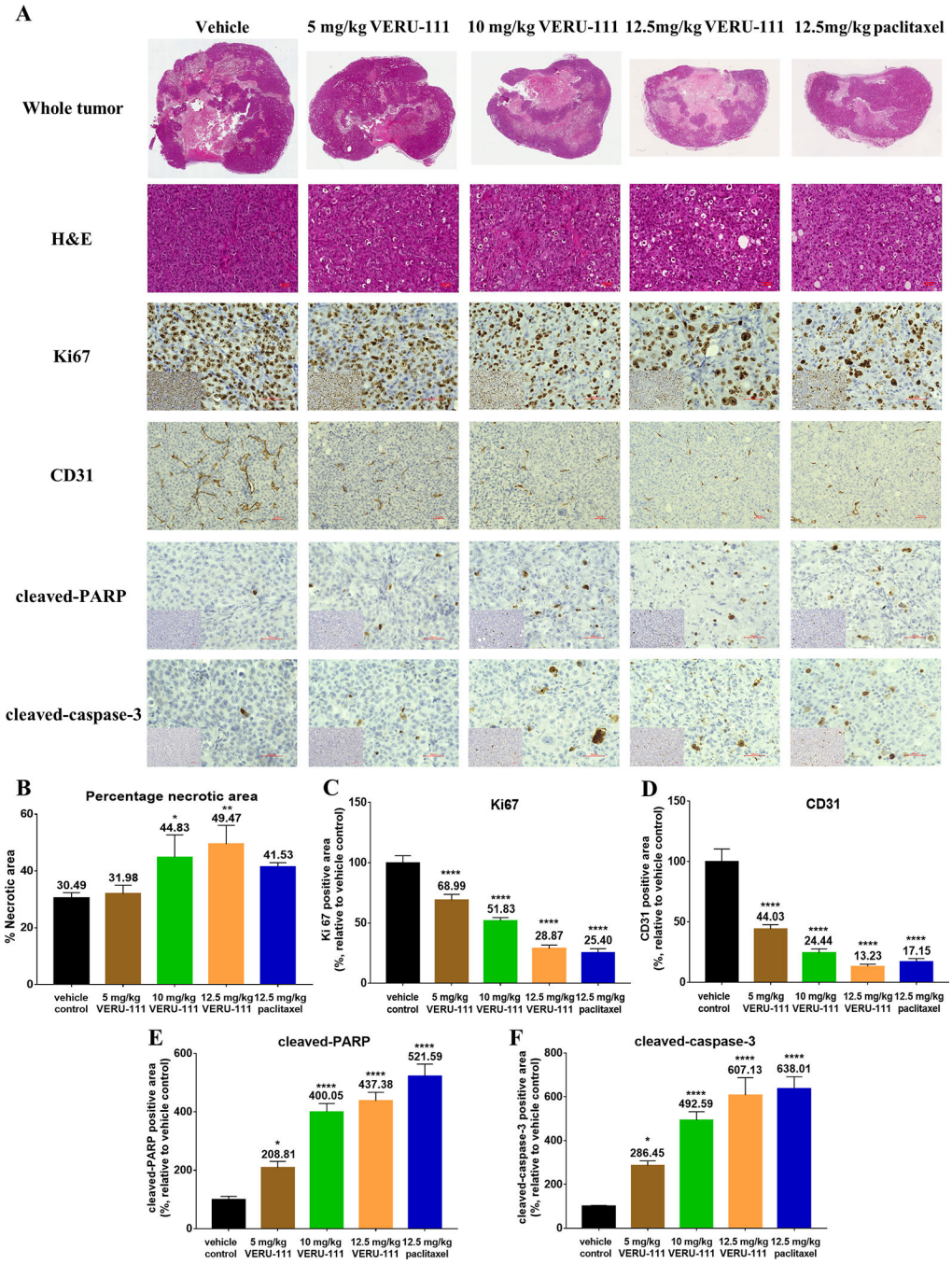

Figure 5.

VERU-111 therapy induces tumor necrosis, represses proliferation and angiogenesis, and induces apoptosis *in vivo*. (A) Representative images of H&E-stained whole tumor sections bisected at the widest width and representative stained slides following immunostaining with Ki67, CD31, cleaved-PARP and cleaved-caspase-3. Images were captured at either 20x or 40x magnification, scale bar = 50 μm. Inserts show low power images. (B) Quantification of the mean percentage of necrotic area ± SEM of H&E sections as scored by an experienced pathologist, expressed relative to the vehicle control. (C-F) Quantification of the mean

percentage ± SEM of Ki67 (C), CD31 (D), cleaved-PARP (E) and cleaved-caspase-3 (F)-positive cells relative to the vehicle control group (100%), the mean value is indicated above each group. All *p*-values are were determined by one-way ANOVA followed by a multiple comparisons test.

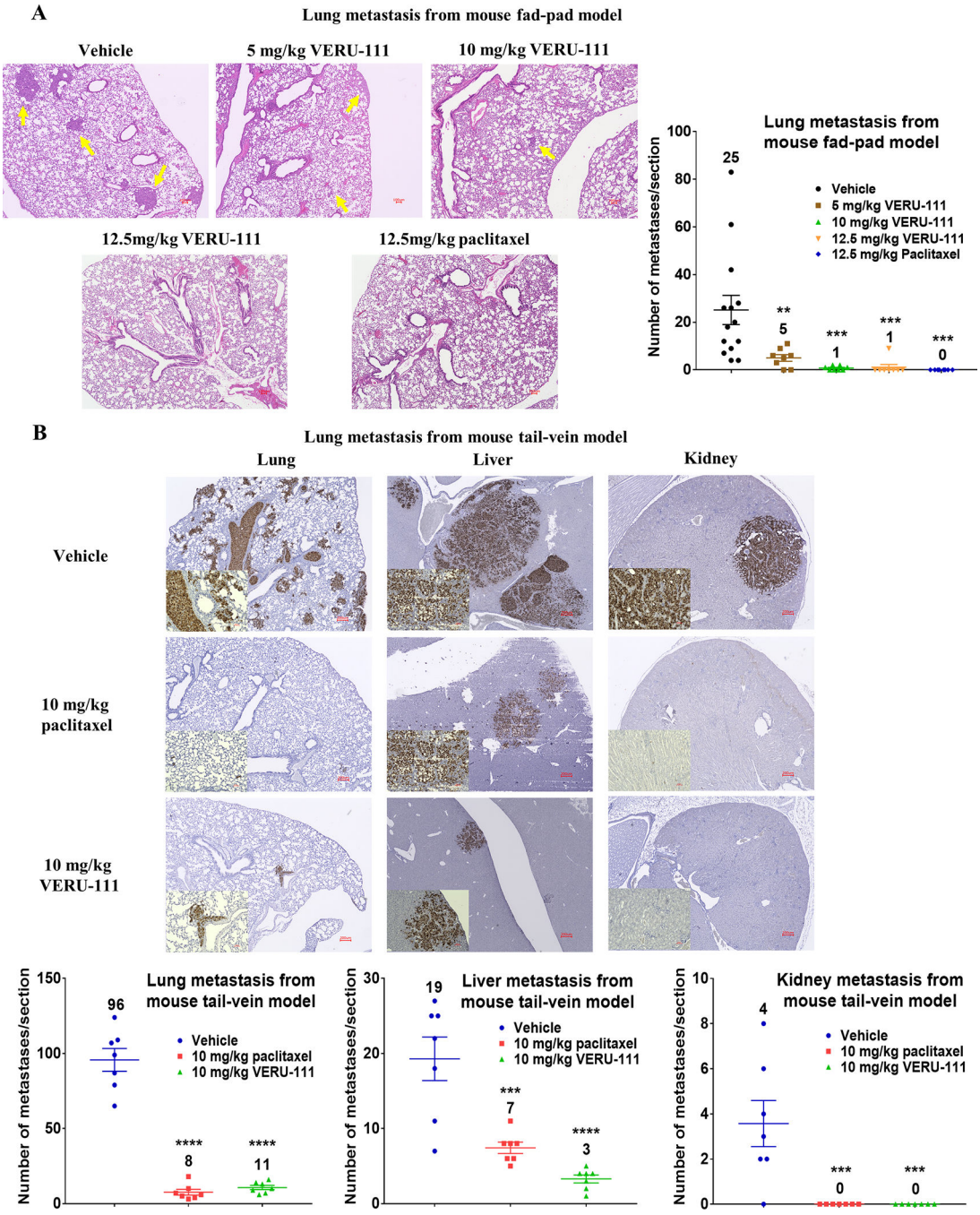

Figure 6.

VERU-111 treatment suppresses metastasis formation in an orthotopic xenograft model and in an experimental lung metastasis model using MDA-MB-231 cells. (A) Representative H&E stained sections of lung metastases derived from orthotopically implanted MDA-MB-231 cells. Lung metastases are indicated by yellow arrows in the H&E-stained slides, 4x magnification, scale bar = 100 μm. Lung metastatic burden of each section from each mouse was quantified after scanning whole slides. (B) Anti-human specific mitochondria IHC staining to detect metastases in lung, liver and kidney sections, scale bar is 200 μm for

primary figures and 50 μm for inserts. Scatter plots of mean ± SEM show the quantification of metastases present in the lung, liver and kidney (A-B). The number above each treatment group correspond to the mean.

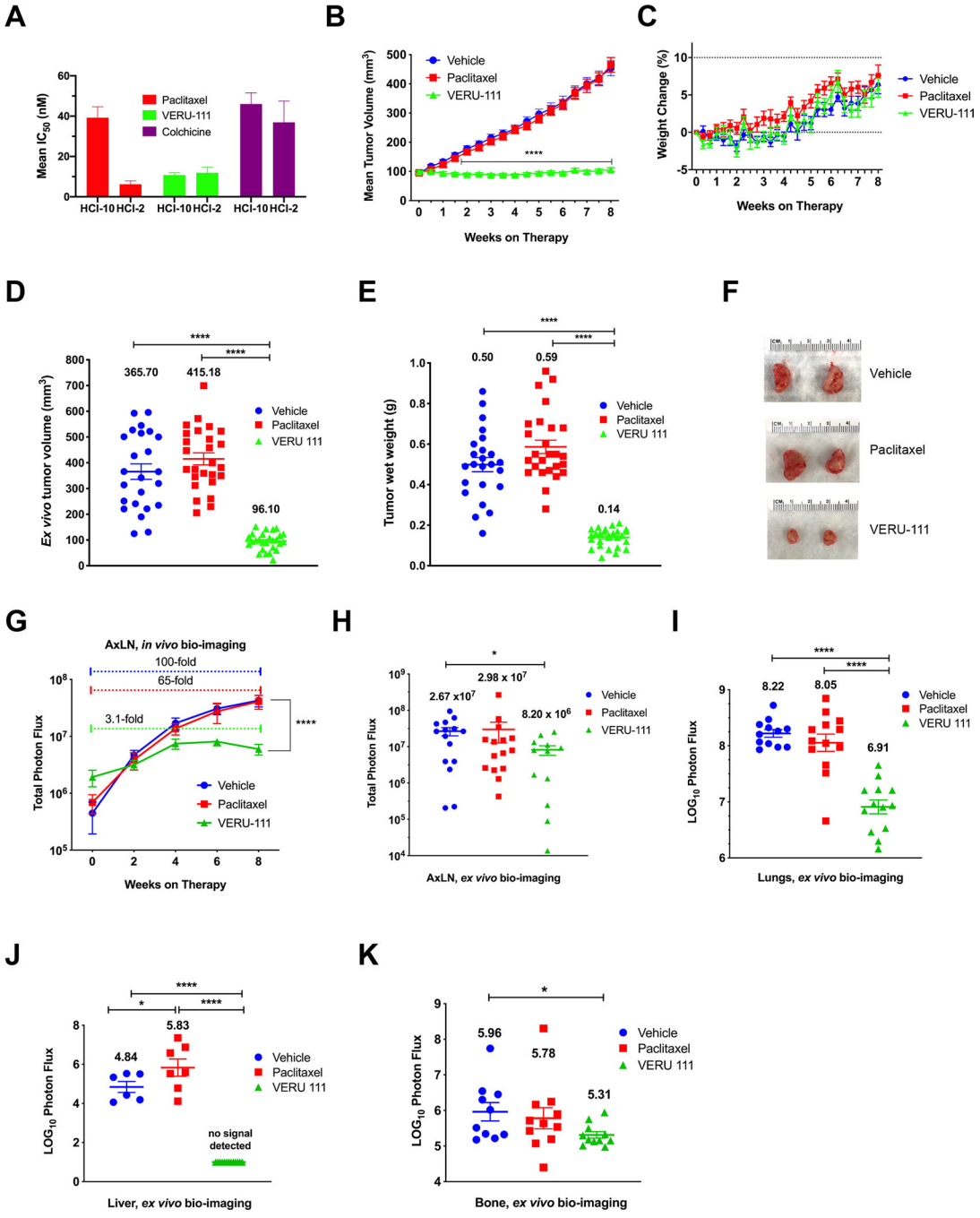

Figure 7.

Antitumor efficacy of VERU-111 in the taxane-resistant HCI-10-Luc2 TNBC xenograft model. (A) Anti-proliferative effect of colchicine, paclitaxel and VERU-111 was measured *in vitro*. The bar graphs represent the grand mean ± SEM of the calculated IC_{50} values from independent drug dosing experiments (n=4) as calculated by the MTS method and validated by IncuCyte S3 live cell imaging (Supplementary Figure S6A). (B) The mean ± SEM tumor volume based on weeks on therapy in response to Vehicle, 10 mg/kg VERU-111, PO (5 times/week) or 10 mg/kg paclitaxel, IP (1x/week). At all-time points beginning at week 1.5

of therapy, the differences between Vehicle or paclitaxel versus VERU-111 are statistically significant; two-way ANOVA followed by multiple comparisons test. (C) Mean percent change in mouse body weight ± SEM during therapy relative to the starting body weight at Week 0. Dashed lines indicate weight decreases below baseline (y axis = 0) and +10% increase in body weight. (D-K) For all experiments, statistically significant differences were determined by one-way ANOVA followed by Dunnett's multiple comparison test at experimental endpoint; only those pairwise analyses that are significant ($p<0.05$) are shown. The cohort mean is shown above each treatment group. For panels G-H, data is plotted on a log-scale along the y-axis, and for panels I-K, $\log_{10}$-transformed data are plotted. (D) Scatter plot of *ex vivo* final tumor volume ± SEM. (E) Scatter plot of final tumor wet weight ± SEM of excised tumors. (F) Images of tumors representative of each group's final tumor volume and wet weight. (G) Mean ± SEM of total photon flux of AxLN metastases present in intact mice one day prior to administration of drug therapy, after assignment to a cohort; data are significant at experimental endpoint between either the vehicle control or the paclitaxel-treated group compared to VERU-111 (solid bracket). The colored dashed brackets compare the baseline AxLN signal of each group from Week 0 to Week 8. (H) Mean ± SEM of total photon flux of AxLN metastases present at experiment endpoint. (I-K) Mean ± SEM of LOG_{10}-transformed total photon flux of lung (I), liver (J) and leg bone (K) metastases as measured *ex vivo* at experiment endpoint. (J) Of note, whereas no signal for liver metastases was detectable in the VERU-111 treatment group, paclitaxel treatment significantly enhanced liver metastasis relative to the Vehicle control.